RSC Advances

ROYAL SOCIETY OF CHEMISTRY

www.rsc.org/advances

RSC Advances

ARTICLE

Decoration of Fe_3O_4 Magnetic Nanoparticles on Graphene Oxide Nanosheets

Received 00th January 20xx,
Accepted 00th January 20xx

DOI: 10.1039/x0xx00000x

www.rsc.org/

M. Bagherzadeh*,[a] M. A. Amrollahi[b] and S. Makizadeh[b]

This study focuses on covalent grafting of Fe_3O_4 magnetic nanoparticles (MNPs) to graphene oxide nanosheets (GNOS) *via* three different chemical routes. To this purpose, firstly, dopamine-functionalized Fe_3O_4 (Fe_3O_4/DA) nanoparticles were firmly attached onto the surface of GONS by activation of carboxciylic groups of GONS *via* thionyl chloride ($SOCl_2$), anhydride formation by using trifluoro acetic acid (TFAA) and 1-ethyl-3-(3-dimethylaminopropyl)carbodiimide/N-hydroxysuccinimide (EDC/NHS) to form Fe_3O_4/DA/GONS. The attachment of Fe_3O_4 MNPs on the GONS surface was evaluated and compared by using FT-IR, XRD, TEM, TGA, VSM, TEM and SAED techniques. The results showed that, depending on the route used, the density and immobilization site of Fe_3O_4 MNPs can be different.

1. Introduction

Graphene, a single-atom-thick nanostructured sheet arranged in honeycomb two-dimensional (2D) lattices, consists of sp^2 hybridized carbon and is considered as a basic building block for graphitic materials of all other dimensionalities [1]. As a "rising-star" carbon material and due to its unique electrical, mechanical, and thermal properties, it greatly promises potential applications in many fields such as nanoelectronics, nanophotonics, catalysis, sensors, nanomaterials, supercapacitors and so on [2,3]. A rapidly increasing interest has been taken recently in graphene oxide (GO), which is strongly oxygenated, highly hydrophilic layered graphene that can be readily exfoliated in water to yield stable dispersions consisting mostly of single layer sheets [4].

However, the prerequisite of such combinations and development applications of the graphene is surface functionalization of the GO. Surface functionalization of the GO not only plays an important role in controlling the exfoliation behavior of GO but also has a key function to entrance in new science and technology gates. The high dispersion stability of graphite oxide enables it to form a single GO layer on many substrates, making it a promising material in functional nanomaterials [5]. The large specific surface area of GO along with its oxygenated functional groups has provided a desired platform for functionalization and loading such nanoparticles as Pd [6], Co_3O_4 [7], quantum dots [8,9], Cu/Ni alloy [10], TiO_2 [11], Au [12], ZnO [13], Fe_2O_3 [14], Fe_3O_4 [15] etc. These nanoparticles have been successfully introduced on the surface or interplane of GO by chemical or physical deposition [16,17]. In general, there are two approaches for surface functionalization of the GO sheets: non-covalent and covalent functionalization [18]. Physical adsorptions or electrostatic interactions used in non-covalent functionalization lead to easy leaching out of functions from GO sheets during application [19]. In addition, it is still a challenge to precisely control the size and location of functions on GO sheets. In covalent functionalization, oxygen functional groups on GO surfaces, including carboxylic acid groups at the edge and epoxy/hydroxyl groups on the basal plane, can be utilized to change the surface functionality of GO [20].

One of the most interesting and practical class of nanomaterials is magnetic nanoparticles (MNPs). The significance of MNPs is owing to their attractive properties and many potential applications in various technologies [21]. Recently, ferromagnetic materials have gained much intense research on biomedical and biotechnological applications. Superparamagnetic iron oxide nanoparticle (Fe_3O_4) is one of the famous magnetic materials in common use. Due to its biocompatibility, catalytic activity, and low toxicity, its applications in biotechnology and medicine have gained significant attention, and it would be promising to merge Fe_3O_4 MNPS properties with GO [22].

Formation of Fe_3O_4/GO is usually achieved by in situ reduction of iron salt precursors, or assembly of MNPs on GO surface, in the same way as its CNT counterpart. Instance decorating Fe_3O_4 MNPs on GO gives Fe_3O_4/GO nanocomposite with promising usages in a variety of fields such as biomedicine, magnetic energy storage, magnetic fluids, catalysis, and environmental remediation [21,23,24]. Produced Fe_3O_4/GO nanocomposites suffer mentioned disadvantages for non-covalent functionalization. On the other hand, covalent functionalizing agents have been previously employed extensively in the surface modification of the sp^2 networks of CNTs [25,26]. Streamline of research shows that the same approach can be applied for the covalent functionalization of

[a] Material Research School, NSTRI, 81465-1589, Isfahan, I.R. IRAN.
[b] Department of Chemistry, University of Yazd, Yazd, I.R. IRAN.
* Corresponding author. E-mail address: mjmo123@yahoo.com (Dr. M. Bagherzadeh).

GO using different kinds of organic modifiers. This target approach, can overcome the mentioned disadvantages of non-covalent functionalization.

Commonly, in order to use carboxylic acid groups to anchor other molecules, carboxylic acid groups have been activated through different activation routes using; *N,N'*-dicyclohexylcarbodiimide (DCC) [27], 2-(7-aza-1H-benzotriazole-1-yl)-1,1,3,3-tetramethyluronium hexafluorophosphate (HATU) [28], 1-ethyl-3-(3-dimethylaminopropyl)carbodiimide (EDC) [29,30], thionyl chloride ($SOCl_2$) [31-34], and by anhydride formation using trifluoroacetic anhydride (TFAA) [35]. The subsequent addition of nucleophilic species, such as amines or alcohols, produces a covalent bond by forming amides or esters. Due to the exciting of abundant carboxylic acid groups on GO, GO becomes a possible starting material for immobilization of a large number of substances including a wide range of metals, biomolecules, fluorescent molecules, drugs, and inorganic nanoparticles. Certainly, due to the capability of the mentioned functionalizing agents, the arrangement and loading of the functions on the surface of GO will be different.

The aim of the present study is to comparatively investigate the abilities of $SOCl_2$, TFAA, and EDC/NHS routes in loading and arrangement of Fe_3O_4 MNPs on the surface of GO. To this end, firstly, Fe_3O_4 MNPs were aminated by using a catechol amine (dopamine, DA). The linkage was based on the chelation of the hydroxyl groups of dopamine with the surface of Fe3O4 nanoparticles, dispersing in water at the same time The amine functions on the attached dopamine allowed for post-covalent bonding of the dopamine-coated magnetic particles (DA/Fe_3O_4) with carboxylic acid derivatives on the GO [36,37]. Then the end amine functional groups of DA/Fe_3O_4 reacted with the carboxylic groups of GO nanosheets (GONS) that were activated *via* $SOCl_2$, TFAA, or EDC/NHS routes, to form Fe_3O_4/DA/GONS. The presence, attachment, loading ability, and decoration of Fe_3O_4 MNPs on the surface of GO *via* these three different routes were evaluated and compared by using FT-IR, XRD, TEM, TGA, VSM, TEM and SAED techniques. The obtained results are presented and discussed later in this paper.

2. Experimental

2.1. Chemicals

Graphite fine powder was used to prepare GO. Ferric chloride hexahydrate ($FeCl_3.6H_2O$), ferrous chloride tetrahydrate ($FeCl_2.4H_2O$), hydrochloric acid (HCl, 37%), and sodium hydroxide (NaOH,) were employed in order to make Fe_3O_4 nanoparticles. 4-(2-Aminoethyl) benzene-1, 2-diol (dopamine, DA) was used for modification of Fe_3O_4 nanoparticles (NPs). Phosphate buffer saline solutions (PBS) in a desired pH and concentration were prepared using Smally's method [38]. Potassium persulfate ($K_2S_2O_8$), phosphorus pentoxide (P_2O_5), sulfuric acid (H_2SO_4, 98%), hydrogen peroxide (H_2O_2, 30%), potassium permanganate ($KMnO_4$), N,N-dimethyl formamide (DMF), $SOCl_2$, TFAA, and EDC/NHS were applied for preparation of GO nanosheets from graphite and its functionalization. All the solutions were prepared with ultrapure water (18 MΩ cm, Millipore-MilliQ, Millipore Inc.). All the materials used in this study were of analytical grades (Merck® except DA from Fluka®)

2.2. Synthesis of graphene oxide nanosheets (GONS)

The GONS was prepared from purified natural graphite using the modified Hummer's method developed as reported in our previous work [39], where graphite powder (5.0 g) was added slowly into a round-bottom flask containing concentrated H_2SO_4 (7.5 mL), $K_2S_2O_8$ (2.5 g), and P_2O_5 (2.5 g) at 80 °C under magnetic stirring. The stirring was continued for 3.5 hours at 80 °C, and then cooled to room temperature naturally. After cooling down to room temperature, the mixture was diluted with deionized water and left for 6 hours. The precipitate mixture was put into 50 mL Teflon tubes, centrifuged at 4000 rpm, then washed successively with deionized water and centrifuged again several times to neutral pH. Finally, the solid was dried under an ambient condition for 1 day. In the second step, concentrated H_2SO_4 (75 mL) was chilled to 0°C by an ice bathroom, and the preoxidized graphite powder (2.5 g) was added and stirred. Then, $KMnO_4$ (7.5 g) was added very slowly under continuous stirring, and the temperature was kept below 10 °C. The mixture was then placed in a water bath at 35 °C and stirred for 2 hours. The mixture was then diluted with deionized water (115 mL) and stirred at room temperature for 2 hours. After that, 350 mL of deionized water and then 30% H_2O_2 (6 mL) were added to the mixture, which changed its color to brilliant yellow. The precipitate mixture was put into 50 mL Teflon tubes and centrifuged at 4000 rpm, then washed successively with a 10% HCl solution, then washed successively with deionized water and centrifuged several times to neutral pH. Finally, the resulting solid was dried at 60 °C for 24 hours where a GONS dark brown powder was obtained.

2.3. Preparation of superparamagnetic Fe_3O_4 NPs

Fe_3O_4 NPs were prepared by chemical coprecipitation methods as reported in our previous works [40,41,42]. First, a solution of HCl (25 mL, 0.4 M) was purged with nitrogen gas for 20 minutes. $FeCl_3.6H_2O$ (5.2 g) and $FeCl_2.4H_2O$ (2.0 g) were dissolved in the solution under a nitrogen atmosphere. Then, the solution was added drop-wise into NaOH (250 mL, 1.5 M) solution under vigorous stirring using a nonmagnetic stirrer at 80 °C. The obtained Fe_3O_4 nanoparticles were separated from the reaction media by a permanent magnet, washed with 200 ml deionized water four times, and then suspended in deionized water (100 ml).

2.4. Preparation of NH_2-functionalized Fe_3O_4 nanoparticles (DA/Fe_3O_4)

DA/Fe_3O_4 nanoparticles were prepared as reported in our previous work [35,40]. Under the nitrogen atmosphere, (0.2 g) was dissolved in a 200 mL phosphate buffer solution (PBS, pH 7.0, 50 mM), and then the resultant solution was ultrasonicated for 30 minutes. Next, MNP suspension (0.2 g) was added to the solution. The mixture was subjected to

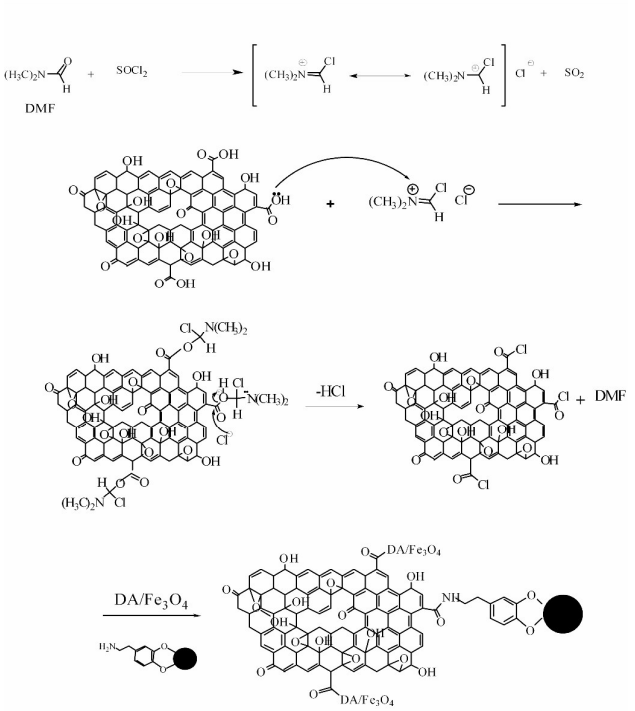

Scheme 1. Schematic representation of the proposed mechanism for synthesis of GONS/DA/Fe_3O_4 by the $SOCl_2$ route.

ultrasonication for 30 minutes at room temperature, and the magnetic nanoparticles were separated from the reaction solution by a permanent magnet, washed with PBS (pH 7.0, 200 mL) for several times, and finally dried at room temperature.

2.5. Preparation of GONS/DA/Fe_3O_4 via $SOCl_2$ route (GONS/DA/Fe_3O_4 ($SOCl_2$))

GONS (0.1 g) was added to a 100 mL round bottom flask containing $SOCl_2$ (50 mL) and *DMF* (3 mL). The mixture was ultrasonicated for 30 minutes and stirred at room temperature for 72 hours. Then, the excess of $SOCl_2$ was evaporated by distillation. After it was washed with anhydrous tetrahydrofuran (THF) and dried at 50 °C in vacuum, a dark powder (GOCl) was obtained. GOCl (0.1 g) was dispersed in THF (200 mL) and sonicated for 30 minutes [16]. Then, the as-prepared DA/Fe_3O_4 (0.1 g) was added to the mixture. After being sonicated for another 30 minutes, the mixture was stirred for 36 hours at room temperature. A dark solid was obtained by removing the solvent under reduced pressure. The crude product was separated by a permanent magnet and washed with anhydrous $C_2H_6Cl_2$ and anhydrous ethyl ether. GONS/DA/Fe_3O_4 ($SOCl_2$) was obtained after it was dried at 50 °C in vacuum (Scheme 1).

2.7. Preparation of GONS/DA/Fe_3O_4 via anhydride formation route (GONS/DA/Fe_3O_4 (TFAA))

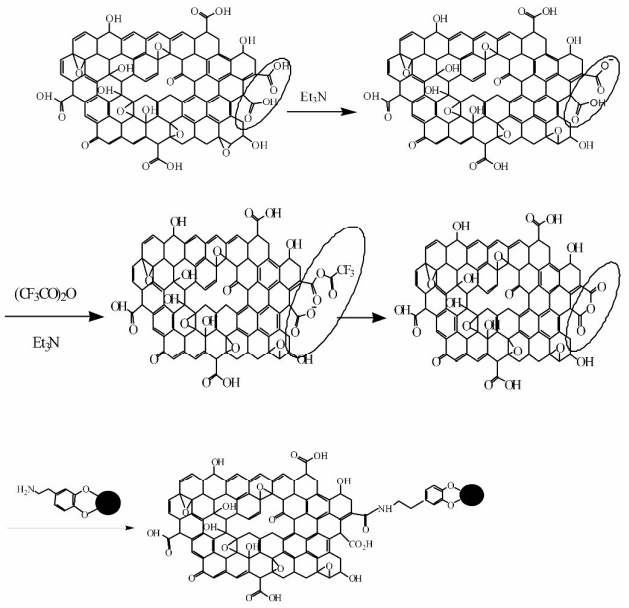

Scheme 2. Schematic representation of the proposed mechanism for synthesis of GONS/DA/Fe_3O_4 by the TFAA route.

First 10 mL trimethylamine (0.64mL) and trifluoroacetic anhydride (0.28 mL) was prepared in anhydrous N,N-dimethylformamide. GONS (0.1 g) was added to the mixture and ultrasonicated for 30 minutes. Then the resultant suspension was stirred for 24 hours at room temperature to activate the carboxylic groups and form a homogenous suspension [35]. Next, DA/Fe_3O_4 (0.1 g) was added to the suspension and stirred for 12 hours. Finally, the resultant was separated by a permanent magnet, washed with water for several times and dried at 50°C in vacuum (Scheme 2).

2.6. Preparation of GONS/DA/Fe_3O_4 via EDC/NHS route (GONS/DA/Fe_3O_4 (EDC/NHS))

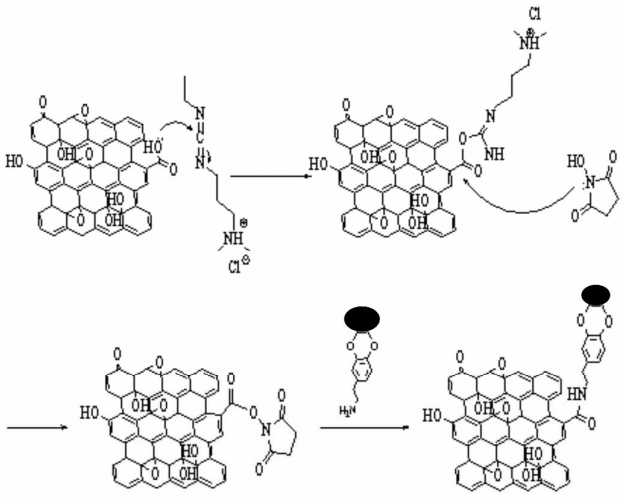

Scheme 3. Schematic representation of the proposed mechanism for synthesis of GONS/DA/Fe_3O_4 by the EDC/NHS route.

GONS (0.1 g) in a 300 ml phosphate buffer solution (pH 7.0, 50 mM), was ultrasonicated for 2 hours, and then EDC (0.05 g) and NHS (0.04 g) were added together to the solution of exfoliated GONS. The mixture was stirred for 1 hour and ultrasonicated for 30 minutes to activate the carboxylic groups and form of a homogenous suspension [29]. Next, DA/Fe_3O_4 (0.1 g) was added to the suspension and the mixture was subjected to ultrasonication for 30 minutes. Finally, the reaction was treated for 30 minutes under stirring using a nonmagnetic stirrer. The GONS/DA/Fe_3O_4 product was separated by a permanent magnet, washed with water for several times and dried at room temperature (Scheme 3).

2.8. Apparatus

Fourier-transform infrared (FTIR) spectroscopy analysis was performed with a Nicolet Impact 400D Model spectrophotometer (Brucker Perkin Elmer Spectrum 65). The crystal structure of the prepared nanomaterials was studied by an X-ray diffractometer (XRD, Bruker Advanced D8 model), using Cu Kα radiation (λ=1.5406A°). The size of the prepared particles was determined using a transmission electron microscope (Philips-EM-208S). The thermal properties of the samples were determined by TGA with a Rhepmetric Scientific STA-1500 using a heating rate of 5 °C/min from room temperature to 1000 °C under an argon atmosphere. The magnetic properties were analyzed using a vibrating sample magnetometer (VSM, Daghigh Meghnatis Kashan Co., Kashan, Iran).

3. Results and discussion

As illustrated in Schemes 1-3, all the synthetic routes of GONS/DA/Fe_3O_4 consist of two steps. First, Fe_3O_4 was modified by DA, and then the amine functional groups of DA/Fe_3O_4 reacted with the carboxylic groups of the graphene oxide nanosheets that were activated *via* different routes to form GONS/DA/Fe_3O_4.

3.1. FTIR;

Fig. 1 shows the FTIR spectra of Fe_3O_4 (a) and Fe_3O_4/DA (b). In the IR spectrum of Fe_3O_4, the peaks at 3400 cm^{-1} and 587 cm^{-1}

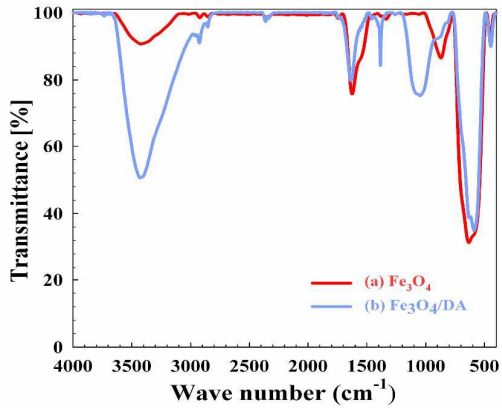

Fig. 1. FTIR spectra of Fe_3O_4 (a) and Fe_3O_4/DA (b).

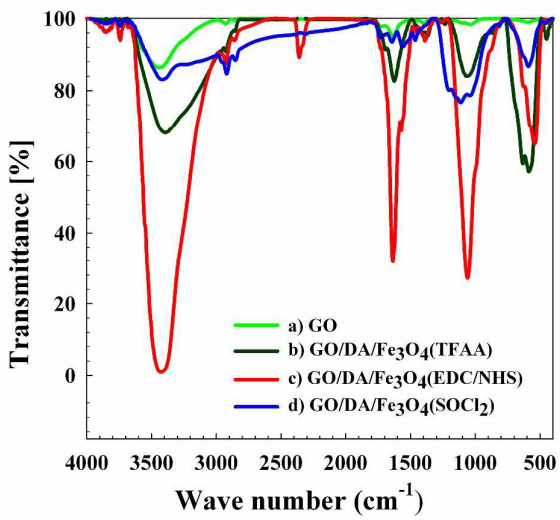

Fig. 2. FTIR spectra of GONS (a), GONS/DA/Fe_3O_4 (TFAA) (b), GONS/DA/Fe_3O_4 (EDC/NHS) (c) and GONS/DA/Fe_3O_4 ($SOCl_2$) (d).

correspond to the hydrogen bonds in water and bending bond of Fe-O respectively (Fig. 1 (a)). The wide absorption at about 1048 cm^{-1} in the Fe_3O_4/DA spectra is attributed to the vibration of C–N bond of Fe_3O_4/DA magnetic particles [35]. Another absorption at 587 cm^{-1} is attributed to Fe–O vibration for the modified Fe_3O_4 [43], confirming the existence of Fe_3O_4 (Fig. 1 (b)). Fig. 2 shows the FTIR spectra of GO and GONS/DA/Fe_3O_4 synthesized by different routes. The observed representative peaks in GO confirm the presence of oxygen-containing functional groups in carbon frameworks (Fig. 2 (a)). The broad peak at 3439 cm^{-1} is ascribed to the stretching of O–H of intercalated water. The C-O stretching vibration of epoxide, the O-H stretching vibration of carboxylic acid, and the C=O stretching of carbonyl and carboxyl groups at the edges of the GO networks are demonstrated by the bonds at 1057, 1220, 1415 and 1728 cm^{-1}, respectively [16]. The peak at 1633 cm^{-1} is attributed to overlapping of the deformation of the O–H bond of the strongly intercalated water absorbed by GO and the aromatic skeletal C=C stretching vibration of the GONS sheets. New bands around 1570 cm^{-1} are attributed to the C-N stretching and the N-H bending vibrations of –CONH groups, the new peak at 1693 cm^{-1} corresponds to C=O stretching of –CONH groups, and the absorption at 581 cm^{-1} corresponds to Fe–O vibration. These observations confirm amide bond formation in the samples [16,19,44] and, consequently, the bonding of Fe_3O_4/DA nanoparticles to the GONS surface can be considered successful. As it can be seen, the intensity of bands around 1570 cm^{-1} shows EDC/NHS > TFAA > $SOCl_2$ order. The difference observed in the case of the band intensity is probably due to the difference among the immobilization routes which contain different leaving groups. Further evidence is needed to confirm the exciting difference among the examined routes.

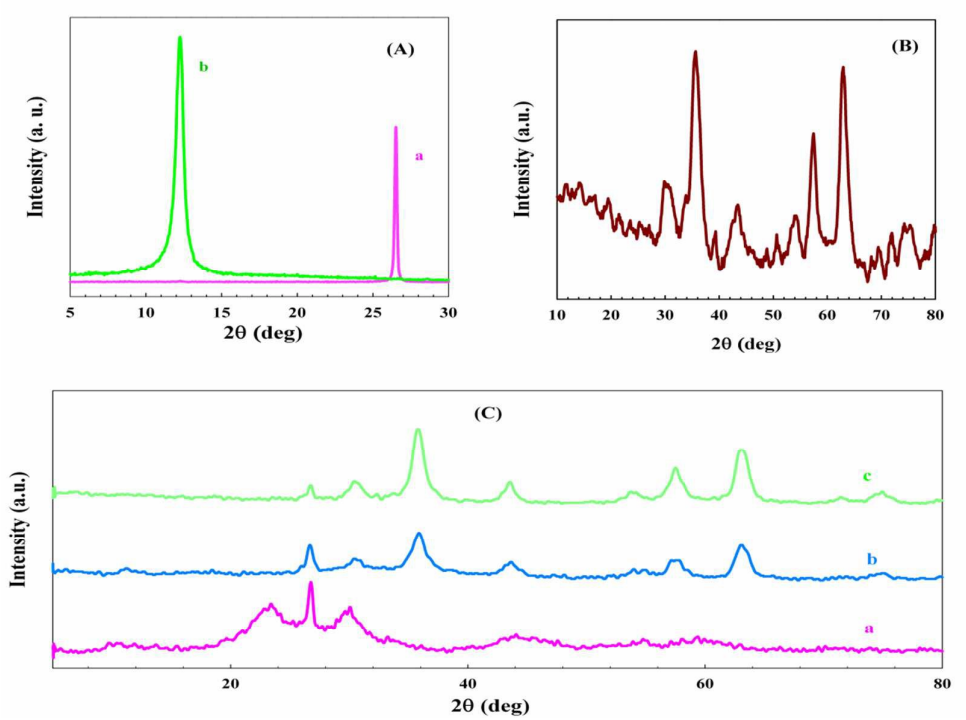

Fig. 3. The XRD patterns of graphite (A-a) and GONS (A-b), Fe_3O_4/DA (B), and (C) GONS/DA/Fe_3O_4 ($SOCl_2$) (C-a), GONS/DA/Fe_3O_4 (TFAA) (C-b) and GONS/DA/Fe_3O_4 (EDC/NHS) (C-c).

3.2. XRD;

The XRD patterns of graphite and GONS are presented in Fig. 3A. Graphite showed a sharp diffraction peak at 2θ=26.5° which could be attributed to the graphitic structure (002) of short-range order in the sample (pattern A-a) that shifted to the lower angle of 12.22° after oxidation. GO showed a sharp peak centered at 2θ=12.22°, which originated from the diffraction on its (002) layer planes (pattern A-b). These data suggest that graphite is successfully converted to GO after oxidation by Hummer's method. The diffraction peaks of the as-synthesized Fe_3O_4/DA particles (Fig. 3B) at 2θ; 18.6, 30.2, 35.6, 43.5, 56.8, and 62.2° are ascribed to the (111), (220), (311), (400), (511), and (440) planes of the magnetite Fe_3O_4, which are in accordance with pure spinel Fe_3O_4 (JCPDS file No. 19-0629) [35]. The XRD patterns of GONS/DA/Fe_3O_4 synthesized from different routes are presented in Fig. 3C. As it can be seen, after surface decoration of GONS by Fe_3O_4 NPs, several new peaks are observed in comparison to paten A-a. The GONS/DA/Fe_3O_4 samples, synthesized from $SOCl_2$ route, showed a diffraction peak at 2θ=25.53° that had resulted from GO, along some low-intensity diffraction peaks indexed to cubic Fe_3O_4 (Fig. 3C-a). Also, the XRD patterns of GONS/DA/Fe_3O_4 samples, synthesized from TFAA and EDC/NHS routes, displayed diffraction peaks at around 2θ=26.70° that had resulted from graphene in the synthesized GONS/DA/Fe_3O_4 structure (Fig. 3C-b and c). The peaks corresponding to the cubic Fe_3O_4 structure, at 2θ; 30.2, 35.6, 43.5, 56.8 and 62.2°, were more intense in case of GONS/DA/Fe_3O_4 synthesized by TFAA and EDC/NHS routes. This is due to its higher concentration of Fe_3O_4 nanoparticles loaded on the surface of GONS (Fig. 3C-b and c).

3.3. TGA;

The thermal behaviors of GONS, Fe_3O_4/DA and GONS/DA/Fe_3O_4 synthesized through different routes are further investigated by thermogravimetric analysis (TGA). As shown in thermogram (a) in Fig. 4, there are four weight loss stages for GO.

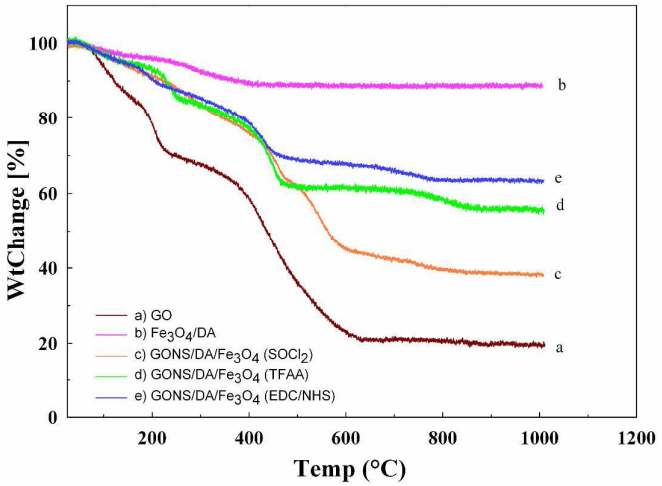

Fig. 4. The TGA curves of GONS (a), Fe_3O_4/DA (b), GONS/DA/Fe_3O_4 ($SOCl_2$) (c), GONS/DA/Fe_3O_4 (TFAA) (d) and GONS/DA/Fe_3O_4 (EDC/NHS) (e).

During the initial heating stage up to 130 ˚C, a 12 % weight loss occurred due to the loss of the water content of the sample and the slow decomposition of the thermally instable GONS. This decomposition speeded up around 180–230 ˚C, where a mass loss (12%) was accompanied by an exothermic reaction. These features correspond to the decomposition of oxygen-containing groups in GONS that are decomposed to carbon dioxide. Abrupt weight loss of 39% takes place around 380–615 ˚C which is attributed to the decomposition of oxygen-containing groups and combustion of the carbon [45]. One can clearly see about an 81 % weight loss of GONS, along with a 19% residual mass at 700 ˚C. Fe_3O_4/DA displayed a small weight loss from room temperature to 120 ˚C (3 wt. %) due to dehydratation. This can be ascribed to the evaporation of surface adsorbed water molecules. It was followed by a weight gain between 250 ˚C and 300 ˚C (16 wt. %) possibly due to the decomposition of dopamine grafted to the Fe_3O_4 surface (Fig. 4 thermogram (b)). The TGA curve of GONS/DA/Fe_3O_4 synthesized by $SOCl_2$ route displayed a small weight loss from room temperature to 420 ˚C due to the loss of the water content of the sample, the slow decomposition of GONS and decomposition of DA grafted to the Fe_3O_4 surface (250-300 ˚C). The weight loss of around 180–230 ˚C, may be attributed to the breakdown of the CONH group conjugated with Fe_3O_4 nanoparticles (Fig. 4 thermogram (c)). The GONS/DA/Fe_3O_4 synthesized by TFAA route exhibit a large weight loss at around 400-460 ˚C, which is attributed to the decomposition of oxygen-containing groups and combustion of carbon (Fig. 4 thermogram (d)). In addition, the GONS/DA/Fe_3O_4 sample synthesized by EDC/NHS route showed the same weight loss at 700 ◦C (Fig. 4 thermogram (d)) [16,46]. The observed results showed, total weight losses about 62, 45 and 37 wt. % for GONS/DA/Fe_3O_4 synthesized *via* $SOCl_2$, TFAA and EDC/NHS routes respectively. By a comparison of the residual mass in thermograms (c-e) with thermogram (a), the contents of MNP were calculated as 19, 36 and 44 %, for GONS/DA/Fe_3O_4 synthesized by $SOCl_2$, TFAA and EDC/NHS routes respectively. The results obtained from TGA technique are in good agreement with the results obtained from FTIR and XRD techniques and confirm a definitely exciting difference between Fe_3O_4 NPs loaded on GONS in EDC/NHS route and the other two routes used.

3.4. VSM;

The VSM magnetization of Fe_3O_4, Fe_3O_4/DA and GONS/DA/Fe_3O_4 synthesized by different routes at room temperature was recorded.

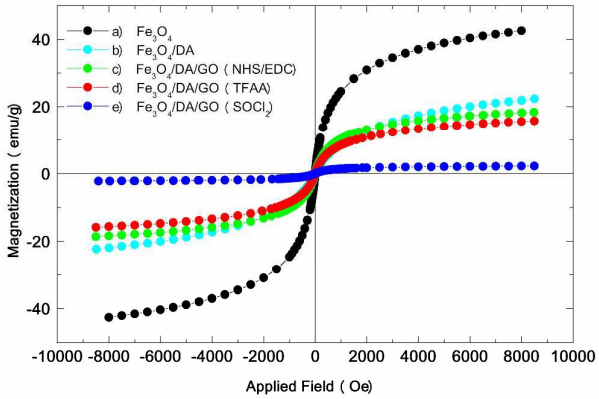

Fig. 5. Magnetic hysteresis loops of the prepared Fe_3O_4 (a) Fe_3O_4/DA (b), GONS/DA/Fe_3O_4 (EDC/NHS) (c), GONS/DA/Fe_3O_4 (TFAA) (c) and GONS/DA/Fe_3O_4 ($SOCl_2$) (d).

As shown in Fig. 5, the magnetization hysteresis loops are S-like curves. The specific saturation magnetization (Ms) as 42.55, 22.31, 18.31, 15.72, and 2.21 emu/g were observed for Fe_3O_4, Fe_3O_4/DA and GONS/DA/Fe_3O_4 synthesized *via* EDC/NHS, TFAA, and $SOCl_2$ routes respectively. All of the magnetic hysteresis had little remanence and coercivity, which demonstrates their superparamagnetic behavior. A comparison of the Ms in Fe_3O_4, Fe_3O_4/DA and GONS/DA/Fe_3O_4 shows a decrease due to addition of a nonmagnetic portion to the Fe_3O_4 magnetic nanoparticles (Table 1). In addition, it is clearly demonstrated in Fig. 5 and Table 1 that the magnetization of GONS/DA/Fe_3O_4 synthesized through EDC/NHS route (18.31 emu/g) is greater than that through other routes, and it is near the magnetization of Fe_3O_4/DA (Table 1). The obtained results from VSM technique are in good agreement with the results obtained from FTIR, XRD and TGA techniques. Also, it is demonstrated that the amount of Fe_3O_4 loaded on GONS has the EDC/NHS > TFAA > $SOCl_2$ order.

3.5. TEM;

The structural size of the synthesis materials were characterized by TEM. Fig. 6 shows the TEM images of GONS (A), GONS/DA/Fe_3O_4 ($SOCl_2$) (B), GONS/DA/Fe_3O_4 (TFAA) (C), and GONS/DA/Fe_3O_4 (EDC/NHS) (D). From Fig. 6A, one can observe that the graphene oxide has a transparent sheet with wrinkled morphology.

Table 1. The values of saturation magnetization (M_s), remanent magnetization (M_r) and coercivity (H_c) of Fe_3O_4, Fe_3O_4/DA and GONS/DA/Fe_3O_4 synthesized from different routes extracted from Figure 5.

Sample	M_s/(emu g^{-1})	M_r/(emu g^{-1})	H_c/Oe
Fe_3O_4	42.55	0.02≈0	2.1
Fe_3O_4/DA	22.31	0.02≈0	1.0
GONS/DA/Fe_3O_4 (EDC/NHS)	18.31	0.02≈0	1.2
GONS/DA/Fe_3O_4 (TFAA)	15.72	0.01≈0	1.1
GONS/DA/Fe_3O_4 ($SOCl_2$)	2.21	0.03≈0	1.3

RSC Advances

ARTICLE

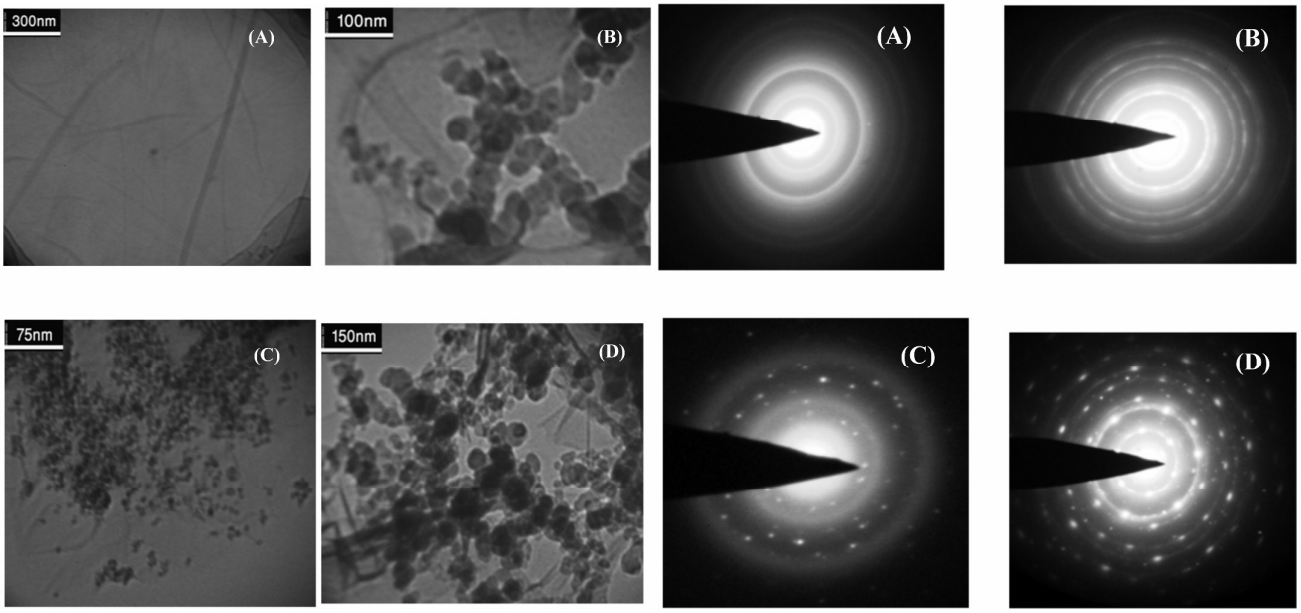

Fig. 6. The TEM images of GONS (A), GONS/DA/Fe_3O_4 ($SOCl_2$) (B), GONS/DA/Fe_3O_4 (TFAA) (C) and GONS/DA/Fe_3O_4 (EDC/NHS) (D).

Fig. 7. The SAED patterns of GONS (A), GONS/DA/Fe_3O_4 ($SOCl_2$) (B), GONS/DA/Fe_3O_4 (TFAA) (C), and GONS/DA/Fe_3O_4 (EDC/NHS) (D).

The TEM images in Fig. 6B-D indicate that Fe_3O_4 NPs are approximately spherical and have been coated on GONS surface. As it can be seen, Fe_3O_4 NPs are firmly attached to GONS, even after the ultrasonication used to pretreat the TEM analysis. However, a closer look at the TEM images proves the density of Fe_3O_4 NPs on the surface of GONS is different and, consequently, depending on the route used, different decorations are observed. The Fe_3O_4 NPs, just arranged on the basal plane (Fig. 6B), are higher than that on the basal plane of GNO (Fig. 6C) and are arranged on both the edge and the basal plane of GONS (Fig. 6D) in the $SOCl_2$, TFAA, and EDC/NHS routes, respectively. Of course, the observed decorations are due to the nature of the routes used for covalent grafting of Fe_3O_4 NPs to GONS. In the $SOCl_2$ route, the activated carboxylic acid groups on the basal planes are more stable and favorable for reaction than those on the edge of GONS. In addition, in the anhydride formation route, TFAA, some of the activated carboxylic acid groups on the edge of GONS have a chance for reaction too, and, consequently, the density of Fe_3O_4 NPs on the surface of GONS is more than that in the $SOCl_2$ route. Also, in the EDC/NHS route, all of the activated carboxylic acid groups on both the edge and the basal plane of GONS are stable and favorable for reaction, and, therefore, the density of Fe_3O_4 NPs on the surface of GONS is higher than that in the other routes. Finally, as Fig 6B-D indicates, among the different synthesis routes, EDC/NHS and TFAA have a high density of Fe_3O_4 NPs on the surface of GONS.

The selected area electron diffraction (SAED) patterns of GONS (A), GONS/DA/Fe_3O_4 ($SOCl_2$) (B), GONS/DA/Fe_3O_4 (TFAA) (C) and GONS/DA/Fe_3O_4 (EDC/NHS) (D), corresponding to the TEM images in Fig. 6, are presented in Fig. 7. The pattern observed in Fig. 7A reveals the polycrystalline and ultrathin structure of GONS. Also, by the SAED patterns in Fig. 7B-D, indicate an interplanar spacing of Fe_3O_4 NPs and graphene, and, a number of diffraction spots are observed in the SAED patterns obtained from the edge of the samples. In addition, there are diffraction spots when moving from the center towards the edge of the samples while the density of those spots differs from sample to sample. Those indicate that the density of Fe_3O_4 NPs on the surface of the GONS in the EDC/NHS route is higher than the other routes. The TEM images and corresponding SAED patterns strongly suggest that the decoration of Fe_3O_4 NPs on the GONS is differing depending selected route.

Conclusions

Herein, Fe_3O_4 magnetic nanoparticles were successfully covalently attached to the graphene oxide nanosheets *via* three different bonding routs. The obtained results show that the decoration and the density of Fe_3O_4 MNPs definitely depend on the applied route. The TEM images prove the obvious difference between the immobilization routs. In conclusion, the density of Fe_3O_4/DA loaded on GONS has an EDC/NHS > TFAA > $SOCl_2$ order. Surely, these results are due to the activity and stability of the activated carboxylic acids *via* deferent routes. While, using $SOCl_2$ and forming acyl chloride is a stronger route to activate carboxylic acid groups, the resulting acyl chlorides are very reactive and unstable, and, unfortunately, $SOCl_2$ route is a hard, toxic and outdated route. On the other hand in the EDC/NHS route, a biocompatible reagent, formation of stable activated carboxylic acid groups leads to an increase in the density of Fe_3O_4/DA loaded on GONS. The results are more important when we come to know that graphene/Fe_3O_4 magnetic nanocomposites have a microwave absorption property [47], and one can tune this property by changing the graphene/Fe_3O_4 ratio. Consequently, the results of this study can help to select an appropriate method of loading Fe_3O_4 or other functionalized nanoparticles on graphene oxide.

Acknowledgements

The authors are strongly grateful to the NSTRI and Yazd University for providing the facilities needed for this study.

References

1 C. N. R. Rao, A. K. Sood, K. S. Subrahmanyam and A. Govindaraj, *Angew. Chem. Int. Ed.*, 2009, **48**, 7752.
2 D. Li and R. B. Kaner, *Science*, 2008, **320**, 1170; D. Li, M. B. Muller, S. Gilje, R. B. Kaner and G. G. Wallace, *Nat. Nanotechnol.*, 2008, **3**, 101.
3 M. Bagherzadeh, S. A. Mozaffari, M. Momeni, *Anal. Methods*, 2015, **7**, 9317.
4 J. I. Paredes, S. Villar-Rodil, A. Martinez-Alonso and J. M. D. Tascon, *Langmuir*, 2008, **24**, 10560; Z. Xing, J. Tian, Q. Liu, A. M. Asiri, P. Jiang, and X. Sun, *Nanoscale,* 2014, **6**, 11659.
5 X. M. Sun, Z. Liu, K. Welsher, J. K. Robinson, A. Goodwin, S. Zaric and H. J. Dai, *Nano. Res.*, 2008, **1**, 203; Z. Liu, J. T. Robinson, X. M. Sun and H. J. Dai, *J. Am. Chem. Soc.*, 2008, **130**, 10876; N. Karousis, A. S. D. Sandanayaka, T. Hasobe, S. P. Economopoulos, E. Sarantopouloua and N. Tagmatarchis, *J. Mater. Chem.*, 2011, **21**, 109; H. J. Jang, Y. K. Kim, H. M. Kwon, W. S. Yeo, D. Kim and D. H. Min, *Angew. Chem., Int. Ed.*, 2010, **49**, 5703.
6 G. M. Scheuermann, L. Rumi, P. Steurer, W. Bannwarth and R. Mulhaupt, *J. Am. Chem. Soc.* 2009, **131**, 8262.
7 C. Xu, X. Wang, J. W. Zhu, X. J. Yang and L. D. Lu, *J. Mater. Chem.*, 2008, **18**, 5625.
8 A. Cao, Z. Liu, S. Chu, M. Wu, Z. Ye, Z. Cai, Y. Chang, S. Wang, Q. Gong and Y. Liu, *Adv. Mater.* 2009, **21**, 103.
9 M. Liu, H. M. Zhao, X. Quan, S. Chen and X. F. Fan, *Chem. Commun.*, 2010, **46**, 7909; A. N. Cao, Z. Liu, Z. Chu, S. S. Chu, M. H. Wu, Z. M. Ye, Z. W. Cai, Y. L. Chang, S. F. Wang, Q. H. Gong and Y. F. Liu, *Adv. Mater.*, 2010, **22**, 103; E. Kaiser, R. L. Colescott, C. D. Bossinger and P. I. Cook, *Anal. Biochem.*, 1970, **34**, 595.
10 S. S. Chen, L. Brown, M. Levendorf, W. W. Cai, S. Y. Ju, J. Edgeworth, X. S. Li, C. W. Magnuson, A. Velamakanni, R. D. Piner, J. Y. Kang, J. Park and R. S. Ruoff, *ACS Nano*, 2011, **5**, 1321.
11 Q. Zhang, Q. An, X. Luan, H. Huang, X. Li, Z. Meng, W. Tong, X. Chen, P. K. Chu, and Y. Zhang, *Nanoscale,* 2015, **7**, 14002; Y. H. Zhang, Z. R. Tang, X. Z. Fu and Y. J. Xu, *ACS Nano*, 2010, **4**, 7303.
12 J. Huang, L. M. Zhang, B. Chen, N. Ji, F. H. Chen, Y. Zhang and Z. J. Zhang, *Nanoscale*, 2010, **2**, 2733.
13 H. X. Chang, Z. H. Sun, K. Y. F. Ho, X. M. Tao, F. Yan, W. M. Kwok and Z. J. Zheng, *Nanoscale*, 2011, **3**, 258.
14 Z. Xing, J. Tian, A. M. Asiri, A. H. Qusti, A. O. Al-Youbi, and X. Sun. *Biosens. Bioelectron.*, 2014, **52**, 452.
15 W. H. Shi, J. X. Zhu, D. H. Sim, Y. Y. Tay, Z. Y. Lu, X. J. Sharma, Y. Zhang, M. Srinivasan, H. Hang, H. H. Hng and Q. Y. Yan, *J. Mater. Chem.*, 2011, **21**, 3422; X. Y. Yang, Y. S. Wang, X. Huang, Y. F. Ma, Y. Huang, R. C. Yang, H. Q. Duan and Y. S. Chen, *J. Mater. Chem.*, 2011, **21**, 3448; G. G. Zhou, D. W. Wang, F. Li, L. L. Zhang, N. Li, Z. S. Wu, L. Wen, G. Q. Lu and H. M. Cheng, *Chem. Mater.*, 2010, **22**, 5306; M. Liu, C. Chen, J. Hu, X. Wu, and X. Wang, *J. Phys. Chem. C*, 2011, **115**, 25234; H. Teymourian, A. Salimi, and S. Khezrian, *Biosens. Bioelectron.*, 2013, **49**, 1; K. Urbas, M. Aleksandrzak, M. Jedrzejczak, M. Jedrzejczak, R. Rakoczy, X. Chen, and E. Mijowska, *Nanoscale Res. Lett.* 2014, **9**, 1.
16 G. Xie, P. Xi, H. Liu, F. Chen, L. Huang, Y. Shi, F. Hou, Z. Zeng, C. Shao, and J. Wang *J. Mater. Chem.*, 2012, **22**, 1033.
17 J. Zhu, T. Zhu, X. Zhou, Y. Zhang, X. W. Lou, X. Chen, H. Zhang, H. H. Hng and Q. Yan, *Nanoscale,* 2011, **3**, 1084.
18 M. Bagherzadeh and A. Farahbakhsh "Surface functionalization of Graphene" in "*Graphene Materials: Fundamental and Emerging Applications*" **2015**, 25-65, USA, Wiley.
19 F. He, J. Fan, D. Ma, L. Zhang, C. Leung and H. L. Chan, *Carbon,* 2010, **48**, 3139.
20 V. Singh, D. Joung, L. Zhai, S. Das, S. I. Khondaker and S. Seal *Prog. Mater. Sci.*, 2011, **56**, 1178.
21 A.H. Lu, E. L. Salabas, and F. Schuth, *Ang. Chem. Inter. Edit.,* 2007, **46**, 1222.
22 Y. Zhang, B. Chen, L. Zhang, J. Huang, F. Chen, Z. Yang, J. Yaoc and Z. Zhang, *Nanoscale*, 2011, **3**, 1446.
23 N. A. Frey, S. Peng, K. Cheng and S. H. Sun, *Chem. Soc. Rev.* 2009, **38**, 2532.
24 M. Nasrollahzadeh, M. Maham, A. Rostami-Vartooni and M. Bagherzadeh, S. M. Sajadi, *RSC Advances*, 2015, **5**, 64769.
25 T. T. Baby and S. Ramaprabhu, *Talanta*, 2010, **80**, 2016.
26 T. Sainsbury and D. Fitzmaurice, *Chem. Mater.*, 2004, **16**, 3780.
27 L. M. Veca, F. Lu, M. J. Meziani, L. Cao, P. Zhang, G. Qi, L. Qu, M. Shrestha and Y. P. Sun, Chem Commun 2009, 2565.
28 N. Mohanty and V. Berry, *Nano Lett.,* 2008, **8**, 4469.
29 R. K. Shervedani, A. Farahbakhsh and M. Bagherzadeh, *Anal. Chim. Acta* 2007, **587**, 254.
30 R. K. Shervedani and M. Bagherzadeh, *Electrochim. Acta,* 2008, **53**, 6293.
31 Y. Xu, Z. Liu, X. Zhang, Y. Wang, J. Tian, Y. Huang, Y. Ma, X. Zhang and Y. Chen *Adv. Mater.* 2009, **21**, 1275.
32 S. Giyogi, E. Bekyarova, M. E. Itkis, J. L. McWilliams, M. A. Hamon and R. C. Haddon, *J. Am. Chem. Soc.* 2006, **128**, 7720.
33 Z. B. Liu, Y. F. Xu, X. Y. Zhang, X. L. Zhang, Y. S. Chen and J. G. Tian, *J. Phys. Chem. B*, 2009, **113**, 9681.
34 H. Yang, C. Shan, F. Li, D. Han, G. Zhang and L. Niu, *Chem. Commun.*, 2009, 3880.
35 M. Bagherzadeh, M. Pirmoradian and F. Riahi, *Electrochim. Acta* 2014, **115**, 573.
36 C. Xu, K. Xu, H. Gu, R. Zhend, H. Liu, X. Zhang, Z. Guo and B. Xu, *J. Am. Chem. Soc.*, 2004, **126**, 9938.

37 A. S. Goldmann, C. Schodel, A. Walther, J. Yuan, K. Loos and A. H. E. Muller, Macromol. *Rapid Commun.*, 2010, **31**, 1608.
38 J. F. Smalley, K. Chalfant, S.W. Feldberg, T. M. Nahir and E. F. Bowden, *J. Phys. Chem. B.* 1999, **103**, 1676.
39 M. Bagherzadeh and M. Heydari, *Analyst*, 2013, **138**, 6044.
40 M. Bagherzadeh, S. Ansari, F. Riahi and A. Farahbakhsh, *International Journal of Electrochemistry,* 2013, (2013).
41 F. Riahi, M. Bagherzadeh and Z. Hadizadeh, *RSC Adv.,* 2015, **5**, 72058.
42 J.-P. Jolivet, C. Chanéac and E. Tronc, *Chem. Commun.*, 2004, 481.
43 Y. Tian, B. B. Yu, X. Li and K. Li, *J. Mater. Chem.*, 2011, **21**, 2476.
44 Y. Zhan, X. Yang, F. Meng, J. Wei, R. Zhao, and X. Liu, *J. Colloid Interface Sci.*, 2011, **363**, 98.
45 A. L. Morel, S. I. Nikitenko, K. Gionnet, A. Wattiaux, J. Lai-Kee-Him, C. Labrugere, B. Chevalier, G. Deleris, C. Petibois, A. Brisson and M. Simonoff, ACS Nano, 2008, **2**, 847.
46 X. Y. Yang, X. Y. Zhang, Y. F. Ma, Y. Huang, Y. S. Wang and Y. S. Chen, *J. Mater. Chem.*, 2009, **19**, 2710.
47 L. Wang, Y. Huang, X. Sun, H. Huang, P. Liu, M. Zong and Y. Wang, *Nanoscale* 2014, **6**, 3157.

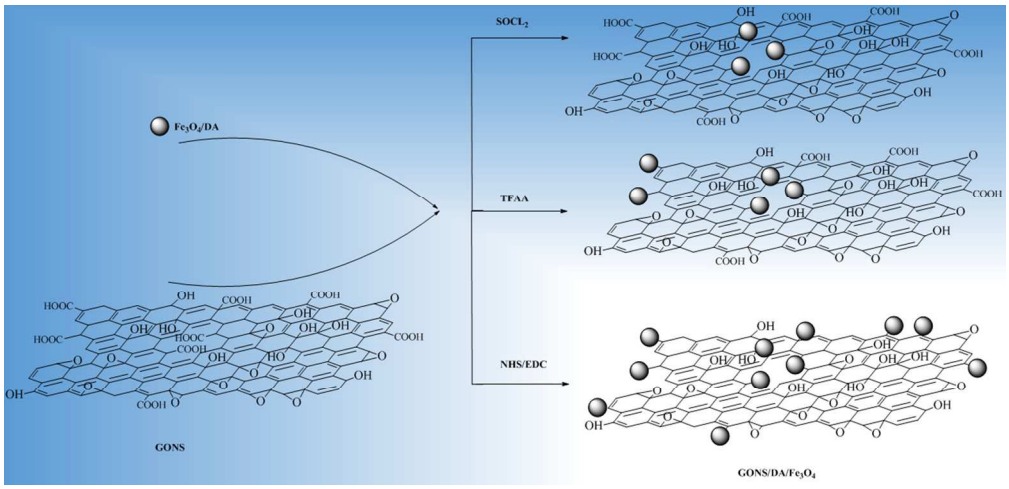

335x160mm (96 x 96 DPI)